Article

Thermally Stimulated Currents in Nanocrystalline Titania

Mara Bruzzi [1,*], Riccardo Mori [2], Andrea Baldi [3], Ennio Antonio Carnevale [4], Alessandro Cavallaro [5], Monica Scaringella [6]

[1] Dipartimento di Fisica e Astronomia, Università di Firenze, Via G. Sansone 1, 50019 Sesto Fiorentino, Firenze, Italy; mara.bruzzi@unifi.it
[2] Albert-Ludwigs-Universität Freiburg, Experimentelle Teilchenphysik, Physikalisches Institut, Hermann-Herder Straße 3, 79104 Freiburg im Breisgau, Germany; riccardo.mori@physik.uni-freiburg.de
[3] Dipartimento di Ingegneria Industriale, Università di Firenze, Via S. Marta 1, 50139 Firenze, Italy; ennio.carnevale@unifi.it, andrea.baldi@unifi.it
[4] LBT Observatory, University of Arizona, 933 N. Cherry Ave, Tucson, AZ 85721, U.S.A.; acavallaro@lbto.org
[5] Dipartimento di Ingegneria dell'Informazione, Università di Firenze, Via S. Marta 1, 50139 Firenze, Italy; monica.scaringella@unifi.it
* Correspondence: mara.bruzzi@unifi.it; Tel.: +39-055-4572291

Abstract: A thorough study on the distribution of defect-related active energy levels has been performed on nanocrystalline TiO_2. Films have been deposited on thick-alumina printed circuit boards equipped with electrical contacts, heater and temperature sensors, to carry out a detailed thermally stimulated currents analysis on a wide temperature range (5-630K), in view to evidence contributions from shallow to deep energy levels within the gap. Data have been processed by numerically modelling electrical transport. The model considers both free and hopping contribution to conduction, a density of states characterized by an exponential tail of localized states below the conduction band and the convolution of standard TSC emissions with gaussian distributions to take into account the variability in energy due to local perturbations in the highly disordered network. Results show that in the low temperature range, up to 200K, hopping within the exponential band tail represents the main contribution to electrical conduction. Above room temperature, electrical conduction is dominated by free carriers contribution and by emissions from deep energy levels, with a defect density ranging within 10^{14} – 10^{18}cm^{-3}, associated to physio- and chemi-sorbed water vapour,OH groups and to vacancy-oxygen defects.

Keywords: thermally stimulated currents; photocurrent; titanium dioxide; hopping; nanoporous film; desorption current; chemisorbed current

1. Introduction

The study of the electronic transport in nanocrystalline Titanium dioxide (nc-TiO_2) is motivated by its wide range of application, from catalysis to green energy systems such as Dye Sensitized Solar Cells (DSSCs) [1] and toxic gas sensing devices [2]. In fact, performances of devices based on nc-TiO_2 strongly depend on electron transport mechanisms, which can be very different from those dominating in the bulk single-crystal semiconductor, due to the complex morphology structure and to the huge active surface of this porous material with respect to its volume. Investigation of the electrical transport properties on nc-TiO_2 and its relationship with surface and bulk defects is thus strategic in the perspective of increasing their performance. A model of the electrical conductivity in nc-TiO_2 that takes into account all the complexities of this material (disorder, fractional dimensionality of the nanoporous material and potential barriers between the constituent nanoparticles) is still lacking; its implementation is a cumbersome task. In order to progress in this

direction, a systematic characterisation of defects states, in the widest range of energy and an evaluation of their concentration in the material is mandatory.

The thermally stimulated current technique is one of the most effective tool for characterizing electrical defects in semiconductors. In this paper, we apply this method to get an overall picture of the defect distribution in nanocrystalline Titania used in state-of-art DSSC devices.

The model of TSC used to interpret our experimental results, takes account of the heavily disordered microscopic nature of nc-TiO_2. In this work, we adopt the model usually considered the for electrical transport in nc-TiO_2 which treats this material as a strongly disordered 3-D medium and neglects the potential barriers at the grain interface; than in general both the hopping and free carrier contributions must be taken into account for the electrical conductivity [3]. In a previous paper a model for the TSC at low temperature was developed starting from studies on strongly disordered semiconductors, such as amorphous semiconductors [4]. In particular, the reference model we considered is that first developed by Gu et al. [3], then extended by Baranovski et al. [5] and Nagy [6] to take into account, in addition to the trapping, the contribution to conduction of hopping electrons, in a variable range model. In our study, previous models have been extended taking into account the degeneracy, a condition that in TSC measurements in disordered media is easily attained either at low temperature or after a strong priming. In this paper, thermally stimulated current analysis [7] is used also to investigate defects related to water, OH groups and vacancy-oxygen, in view to give a quantitative contribution to elucidate their role in transport properties, nowadays still a matter of intense debate [8,9].

2. Mixed conduction model in nc-TiO_2

In heavily disordered semiconductors, significant carrier hopping can occur between localized sites, whose energies fall within the band gap, giving a non-negligible contribution to the electrical conductivity. As a result, mixed conduction mechanisms with hopping and free carriers contributions should be taken into account when discussing the electrical transport in such a material, especially at low-to-moderate temperatures and high carrier densities.

As it is usually done, we consider the nc-TiO_2 as a strongly disordered intrinsic semiconductor whose charge carriers are electrons: then the Density of States (DoS) is modelled as the sum of the extended state contribution (i.e. the conduction band), with the typical square root dependence on energy, and the localized state contribution characterized by an exponential tail, below the conduction band, as for amorphous materials [10]. Then, the density of states in the overall energy range, putting at ε = 0 the border between extended and localized states, is given by the function:

$$g(\varepsilon) = \frac{N_L}{E_L}\,\theta(-\varepsilon)e^{\frac{\varepsilon}{E_L}} + \theta(\varepsilon)N_{C0}\sqrt{\varepsilon + E_B}, \quad (1)$$

with $\theta(\varepsilon)$ Heaviside function, E_L tailing factor, $N_L = \int_{-\infty}^{0} g(\varepsilon)d\varepsilon$ total density of localized states within the band gap, N_{C0} related to the effective density of states at the conduction band minimum (N_{C0} = 4 10^{19} $cm^{-3}meV^{-3/2}$, in order to get at room temperature N_C = 5.2 10^{21} cm^{-3}, typical for TiO_2). The energy parameter:

$$E_B = \left(\frac{N_L}{N_{C0}E_L}\right)^2, \quad (2)$$

is introduced so as to have the continuity of $g(\varepsilon)$ at ε = 0. The DoS obtained with this procedure is shown in Figure 1.

Preprints (www.preprints.org) | NOT PEER-REVIEWED | Posted: 1 November 2017 doi:10.20944/preprints201711.0002.v1

Peer-reviewed version available at Nanomaterials 2018, 8, 13; doi:10.3390/nano8010013

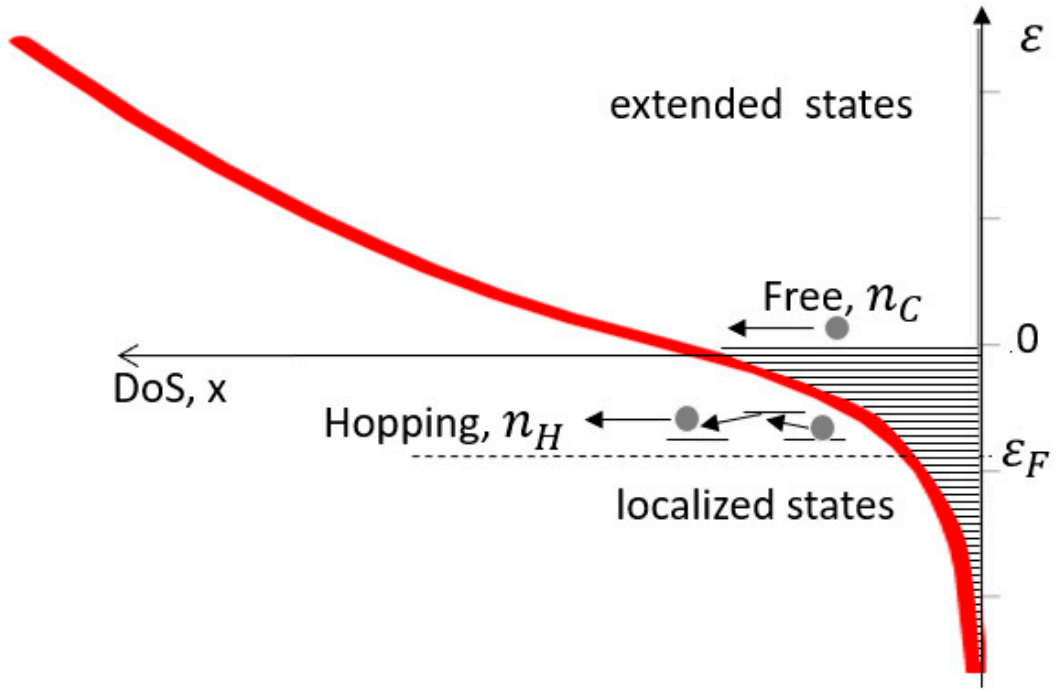

Figure 1. DoS as obtained with an exponential decay tail in the forbidden gap and a square root dependence in the conduction band region. The boundary is kept at ε_C = 0, minimum of the conduction band. conduction is due to both free electrons in the conduction band and to hopping at localized states.

Mixed electrical conductivity, in case of a n-type nc-TiO_2 layer, is the result of transport processes of both hopping electrons within the band tail and free electrons in the conduction band, as depicted in figure 1, then for the total conductivity we have:

$$\sigma = \sigma_H + \sigma_C = q\mu_H n_H + q\mu_C n_C, \tag{3}$$

where σ_H and σ_C, μ_H and μ_C, n_H and n_C, are conductivity, mobility and electron concentration of hopping carriers and free carriers respectively; q is the electron charge. In (3) μ_H is an effective mobility that must be calculated taking into account that the hopping probability depends on the site. Assuming the validity of the Einstein relation, the hopping mobility is related to the carrier energy through the diffusivity $D(\varepsilon)$:

$$\mu(\varepsilon) = \frac{q}{K_B T} D(\varepsilon) = \frac{q}{K_B T} \mathrm{r}(\varepsilon)^2 \nu, \tag{4}$$

with ν hopping rate and r(ε) average distance between hopping sites available for hopping for carrier with energy ε. The rate for hopping from site i to site j, respectively characterized by energies ε_i and ε_j, is given by the Miller-Abrahams [11] model:

$$\nu = \nu_0 \begin{cases} e^{-2\frac{r_{ij}}{\alpha} - \frac{\varepsilon_j - \varepsilon_i}{K_B T}}, \varepsilon_i < \varepsilon_j \\ e^{-2\frac{r_{ij}}{\alpha}}, \varepsilon_i > \varepsilon_j \end{cases}, \tag{5}$$

where r_{ij} is the distance between sites at ε_i and at ε_j, α is the localization radius of the electron and ν_0 is the hopping frequency coefficient.

The localization radius can be assumed as a constant, of the order of a few angstrom, for states deeply localized, but when approaching the boundary ε = 0 with the extended states this length diverges. Then, as the hopping probability depends exponentially on this length, the description of the conduction for carriers localized in states near the mobility edge must take into account this behavior. This divergence, according to several models, behaves as $E^{-\gamma}$ with γ ranging between 0.5 and 1.5 [10]. Here, we assume for the localization length α:

$$\alpha(\varepsilon) = \alpha_0 \left(1 - \frac{z}{\varepsilon}\right)^{\gamma}, \tag{6}$$

with α_0 carrier localization length of the deep states and z the energy to which α starts to diverge. The evaluation of the hopping conductivity requires some kind of approximation in order to get an expression useful for fitting experimental data. Referring to the approach already proposed by Nagy [6] the hopping conductivity can be calculated as:

$$\sigma_H(T) = q \int \mu \; dn \; = \nu_0 \frac{q^2}{K_B T} \int_{-\infty}^{0} g(\varepsilon) f(e, E_F, T) r(\varepsilon)^2 e^{-2\frac{r(\varepsilon)}{\alpha(\varepsilon)}} d\varepsilon, \tag{7}$$

where $r(\varepsilon)$ is an average hopping distance for a site of energy ε, given by:

$$\frac{1}{r(\varepsilon)^3} = \frac{4\pi}{B R_L^3} \int_{-\infty}^{\varepsilon} g(\varepsilon')[1 - f(\varepsilon', E_F, T)] d\varepsilon',$$
$$\frac{1}{{R_L}^3} = \frac{4\pi}{3} \int_{-\infty}^{0} g(\varepsilon') d\varepsilon' = \frac{4\pi}{3} N_L \,, \tag{8}$$

with $f(\varepsilon, E_F, T) = \frac{1}{1+e^{\frac{\varepsilon - E_F}{K_B T}}}$, Fermi-Dirac distribution function and B the percolative limit factor, namely the average number of site links, a parameter dependent on the system dimensionality (B=2.7 for 3-D hopping [5]).

The Fermi energy E_F is obtained by evaluating the total electron concentration n as the sum of the electron density in the band tail (ε<0), n_H, and in the conduction band (ε>0), n_c; then $n = n_C + n_H$, where:

$$n_H = \int_{-\infty}^{0} g(\varepsilon) f(e, E_F, T) d\varepsilon \quad , \quad n_c = \int_{0}^{\infty} g(\varepsilon) f(e, E_F, T) d\varepsilon. \tag{9}$$

Finally, the contribution of free electrons to the electrical conductivity is given by the typical expression of the conductivity for electrons in the conduction band:

$$\sigma_c(T) = q \mu_c n_c = q \frac{\mu_{c0}}{(K_B T)^{3/2}} n_c, \tag{10}$$

with n_c as calculated from Eq. 9. A typical value for the TiO_2 mobility constant is μ_{c0} = 1 $cm^2 meV^{3/2}/Vs$, which gives a room temperature mobility μ_c = 7.5 10^{-3} cm^2/Vs [13].

3. Rate equations for priming and thermally stimulated process

The rate equation for hopping and free carriers is:

$$\frac{dn}{dt} = -\left(\frac{dn_H}{dt}\right) - \frac{n_C}{\tau_C} + S(t), \tag{11}$$

where $S(t)$ is the generation rate during priming (e.g. light exposure, null during the TSC scan). Here conduction carriers decay is considered via annihilation on recombination centers or trapping from deep levels, characterized by an active energy level within the gap. The free electron lifetime, τ_C, is typically dependent on the defect capture cross section σ_t and concentration N_t:

$$\frac{1}{\tau_c} = N_t \sigma_t < v_{th} >= N_t \sigma_t \sqrt{\frac{3K_B T}{m}}, \tag{12}$$

where m is the effective mass of the free carriers (in TiO_2 it is about 7 times the electron mass m_0 [12]) and $< v_{th} >$ their average thermal velocity. In general, in a disordered semiconductor, defects may have a spread in energy, so its concentration is calculated through a gaussian distribution:

Peer-reviewed version available at Nanomaterials 2018, 8, 13; doi:10.3390/nano8010013

$$N_t = \frac{N_{t0}}{\sqrt{2\pi}\,\sigma_{E_t}} \int e^{-\frac{(\varepsilon - E_t)^2}{2\sigma_{E_t}{}^2}} d\varepsilon, \tag{13}$$

The decay of the hopping carriers, in turn, is given as [5]:

$$\left(\frac{dn_H}{dt}\right)_{dec} = -\int_{-\infty}^{0} \frac{g(\varepsilon) f(\varepsilon)}{\tau(T,\varepsilon)} d\varepsilon, \tag{14}$$

$$\frac{1}{\tau(T,\varepsilon)} = N_t \frac{r(\varepsilon)^2 D(\varepsilon)}{\alpha} = \nu_0 N_t \frac{r(\varepsilon)^4}{\alpha} e^{-2\frac{r(\varepsilon)}{\alpha}}. \tag{15}$$

In the following, we will describe results of decayed/fractionated Thermally Stimulated Currents (TSC) experiments analyzed with the mixed conduction model described above. In this method, after priming the sample only once at a low temperature, successive cycles of heating/cooling are applied to fractionally deplete levels of lowering energy. The sample is heated up to a first maximum temperature T_{stop} and cooled down to a first minimum temperature T_{start} then it is heated and cooled again to higher T values and so on, eventually up to the final temperature.

At first, we have used the decayed TSC method to get useful information about the DoS shape. For each scan of the decayed TSC, we extracted the couple (E_{act}, Q) with E_{act} = activation energy as determined from the initial rise of the TSC and Q = emitted charge calculated by integrating the TSC of the corresponding scan [15]. In this way, we obtained the DoS shape as a function of the energy by plotting the charge released at each step as a function of the activation energy E_{act}.

Then, delayed TSC measurements have been best fitted using the mixed conduction model, considering a constant heating/cooling rate: $\beta = \frac{dT}{dt}$, starting from the initial condition due to priming, stated that in between two scans there is a time delay in which the electrical state of the sample evolve very slowly. So, assuming the initial state got from priming, it is possible to fit the entire sequence of the delayed TSC at once. The rate equation is solved starting from an evaluation of the Fermi level, then the distance between hopping sites, the transport energy, the hopping carrier density and the average hopping rate are obtained and finally iterating for each temperature the calculation is performed for the entire experimental data set.

In the high temperature range, above room temperature, when conductivity is mainly due to free carriers and hopping can be neglected, in our model TSC is considered as dominated by deep centers with discrete energy levels E_t in the forbidden gap, characterized by a capture cross section σ_n (for electrons) and a trap N_t concentration. So, we consider the standard TSC expression as [16]:

$$I_{TSC}(T) = q\mu_c \Sigma N_t F e_n(T) e^{-\frac{1}{\beta}\int_{T_i}^{T} e_n(T) dT}, \tag{16}$$

with $e_n(T) = N_C \sigma_n v_{th} e^{-\frac{E_C - E_t}{K_B T}}$ emission constant, Σ surface normal to electric field F, T_i initial temperature of the scan Due to the disorder in the nanocrystalline material, the TSC peak usually results in a peak broader in temperature than the standard one. This is due to the fact that the energy E_t of a defect varies within a certain range due to local morphological changes. We have taken into account that by convoluting the TSC peak with a gaussian distribution, as given in Eq. 13.

4. **Experimental Set-up and Procedure**

To manufacture our samples, we used a colloidal system produced by Solaronix, Switzerland, containing about 11 % wt. nanocrystalline titanium dioxide mixed with optically dispersing anatase particles (13/400 nm, Ti-Nanoxide D). This material is specifically developed for prototypal electrodes in DSSCs. We deposited the nc-TiO_2 paste on alumina substrates having two parallel gold contacts, 7mm long and spaced 0.8mm; thickness of the film is about 1 µm. A picture of the sample is shown in Fig. 2. After deposition, the films have been syntherized in two steps, 30 minutes each, first at 280 °C and then at 450°C. The current-voltage characteristics of the sample showed an ohmic behaviour in the overall investigated range (0-100V) with room temperature resistivity of the order of 2×10^8 Ωm [15]. In a typical DSSCs, with a 2µm-thick nc-TiO_2 film, a voltage of about 0.5V is applied and an average electric field of about 2.5×10^5 V/m is settled. In our TSC measurements we therefore chose to

Peer-reviewed version available at Nanomaterials 2018, 8, 13; doi:10.3390/nano8010013

apply a bias of 100V across the sample, in view to get an electric field of the same order of magnitude, considering the increased distance between our planar electrodes.

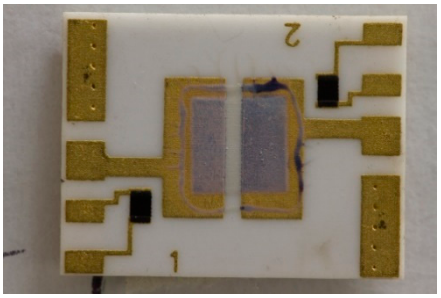

Figure 2. Nc-TiO_2 film deposited on an alumina chip for TSC measurements.

To perform TSC measurements in the temperature range 5-300K, the alumina substrates coated with the nc-TiO_2 have been placed in a sample holder equipped with a 4Ω heating resistor and a silicon temperature sensor. The sample-holder has been inserted into a dewar containing liquid He (LHe) and positioned over the LHe vapours to ensure stable temperatures down to 4.2K, minimize thermal inertia and reduce possible mismatch between the sample and the thermometer. Details of the experimental setup are given in [16]. Polarization of the sample and current reading was performed by a Keithley 6517 electrometer, the heater was biased by a TTi QL564P power supply and temperature was read by a Lakeshore DRC91C temperature controller. Priming was performed by a LED source placed in front of the sample inside the sample holder. We used two priming sources: a 400 nm UV (NUV) LED and a 355 nm UV (FUV) LED, having 12 mW (typical) and 8.4 mW (maximum) output power, respectively. LEDs were driven by a Systron Donner 110D pulse generator. The light spot on the sample during illumination has a diameter of about 2mm.

Delayed TSC measurements have been performed as follows. We primed the sample at a low temperature T_0 with the LED source, biasing the sample at 100 V. Then, we waited a time interval to make fast transient effects relaxing and to get a constant temperature on the whole sample. Then, fractionated TSC analysis has been carried out performing different heating/cooling cycles up to 300K. TSC has been also studied in the temperature range from 300K to 630K using a different chamber where heating / cooling is performed by a system controlling temperature, pressure and gas composition. During each TSC measurement, both in the low and high temperature ranges, the scan rate was fixed at 0.1 K/s.

5. Experimental Results and Discussion

Figure 3 shows a typical TSC spectrum observed in the overall range 5-630K obtained with the procedure described in the previous section. A fractionated TSC is performed up to 300K, after priming at 5K. Then, a second priming is carried out at 300K inside the high temperature TSC setup and a second TSC analysis is performed up to 630K. The low temperature analysis is divided into 4 TSC fractions in the ranges: 5-20K, 20-80K, 80-180K, 180-300K, then, a unique TSC curve is measured after priming at 300K up to 630K. At last, a final cooling step from 300 to 250K is measured to close the whole cycle.

Preprints (www.preprints.org) | NOT PEER-REVIEWED | Posted: 1 November 2017 doi:10.20944/preprints201711.0002.v1

Peer-reviewed version available at Nanomaterials 2018, 8, 13; doi:10.3390/nano8010013

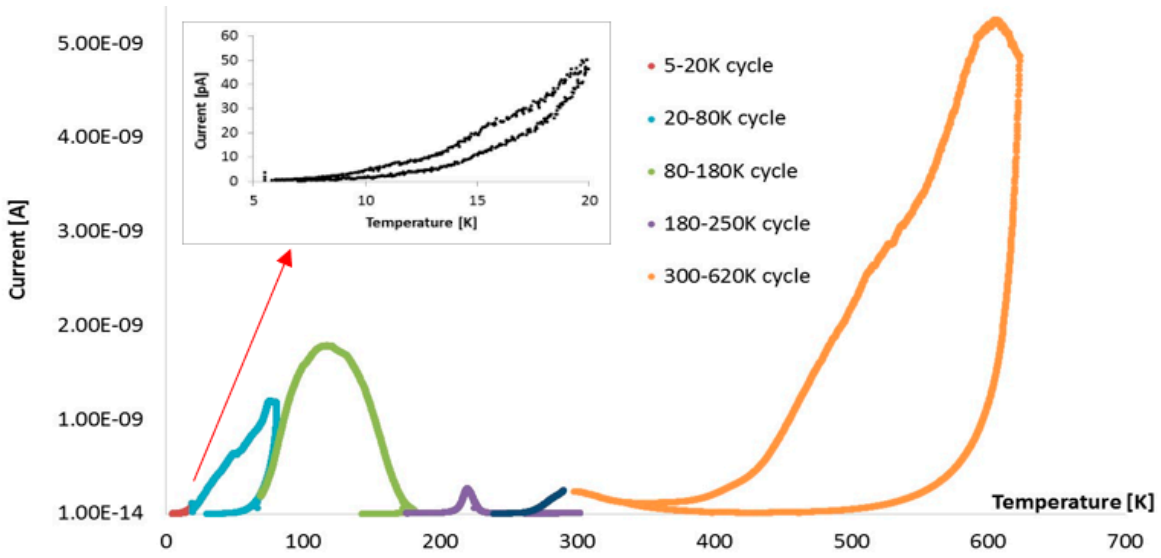

206 **Figure 3.** Fractionated TSC analysis performed in different cycles of measurements after UV priming
207 at 5K. Inset on the left shows an enlarged view of the 5-20K temperature range.

208 Main conductivity processes in the two temperature ranges 5-300K and 300-630K are different.
209 In fact, in the low T range, hopping conduction is non- negligible against free conduction. Conversely,
210 in the high T range conductivity is mainly due to free carriers. Moreover, in this latter case, the
211 influence of the surrounding gas atmosphere to the charge state of deep discrete levels in the
212 forbidden gap cannot be neglected. Thus, in the following, we will discuss separately results
213 measured below and above room temperature.

214 *5.1. TSC analysis below room temperature*

215 Figure 4 compares the TSC spectrum measured in the low T range together with TSC data
216 reported in past for single crystal TiO_2 [19].

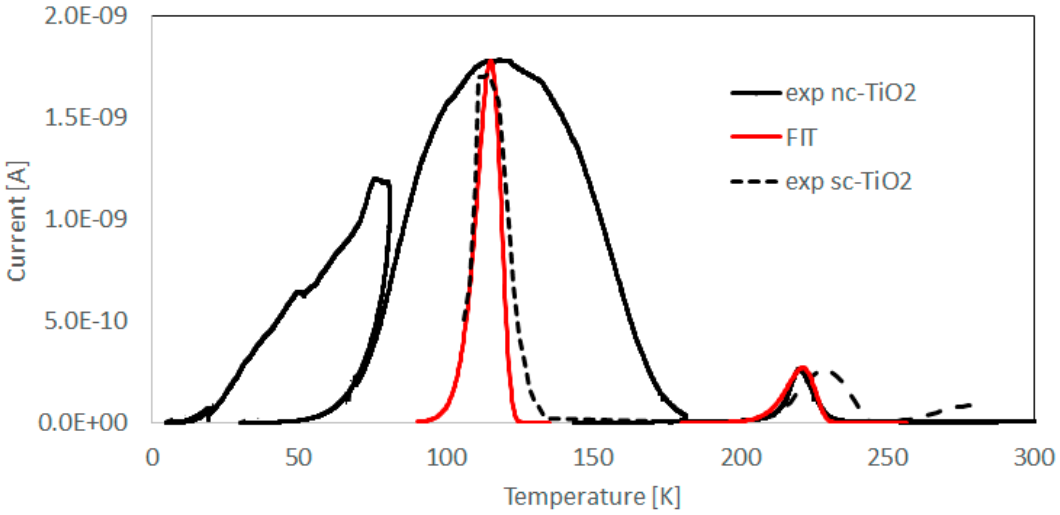

217 **Figure 4.** Fractional TSC measured with the nc-TiO2 film in the range 5-300K compared with
218 experimental TSC peaks reported in [19] for single crystal TiO_2 and with a best fit obtained
219 considering a standard TSC emission from discrete energy levels. The experimental peaks for sc-TiO_2
220 have been multiplied respectively by 1700 (120K) and 500 (230K) to compare with those measured
221 with the nc-TiO_2 ones.

Preprints (www.preprints.org) | NOT PEER-REVIEWED | Posted: 1 November 2017 doi:10.20944/preprints201711.0002.v1

Peer-reviewed version available at Nanomaterials 2018, 8, 13; doi:10.3390/nano8010013

In single crystal TiO_2, two peaks related to two discrete energy levels at 120K and 230K are present, which can be described in terms of standard TSC emissions [16] as given in Eq. 16. In nanostructured TiO_2, we observe a much broader peak at 120K, which cannot be described in terms of standard single-level TSC emission, and a peak at 220K, rather similar to the one measured in single crystal TiO_2. In the figure, a best fit of this latter peak is shown, obtained with a standard TSC analysis (Eq. 16), a very high capture cross section, $\sigma_n \approx 10^{-10}$ m^2 and $E_t \approx 0.8$eV, $N_t \approx 10^{14}$cm^{-3}.

To investigate the origin of the broad band peaked at 120K, we then performed a measurement in the same temperature range with more delayed heating steps (up to 10). Results are shown in the inset of figure 5. We note that, in a standard thermally activated emission where carriers are emitted from discrete energy levels towards the corresponding extended band, the current measured at the foot of the TSC curve in each heating / cooling step has a dependence on temperature given by: $I(T) \propto T^2 e^{-\frac{E_{act}}{K_B T}}$, while if hopping conduction dominates, the dependence should be (Mott's expression): $I(T) \propto e^{-\left(\frac{T_0}{T}\right)^4}$ [20]. Inset of fig. 5 shows current measured in the range 5-150K in a Mott plot. Indeed, the foot of the logarithmic plots at each heating/cooling stage is linear with $T^{-1/4}$, in agreement with the fact that hopping conduction is prevailing in this temperature range and that, as suggested by [4], it should be related to a band tail deforming the DoS shape close to the mobility edge.

As described in the previous section, to investigate the DoS shape we evaluated, for each scan, the activation energy in the rising foot range of each peak and the corresponding total emitted charge. The result is shown in Fig. 5, where the total charge is plotted as a function of the activation energy. Results evidence a mono-exponential DoS: $f(\varepsilon) = Q_L e^{\frac{\varepsilon}{E_L}}$(E), in the energy range 0.1-0.6eV with E_L tailing factor.

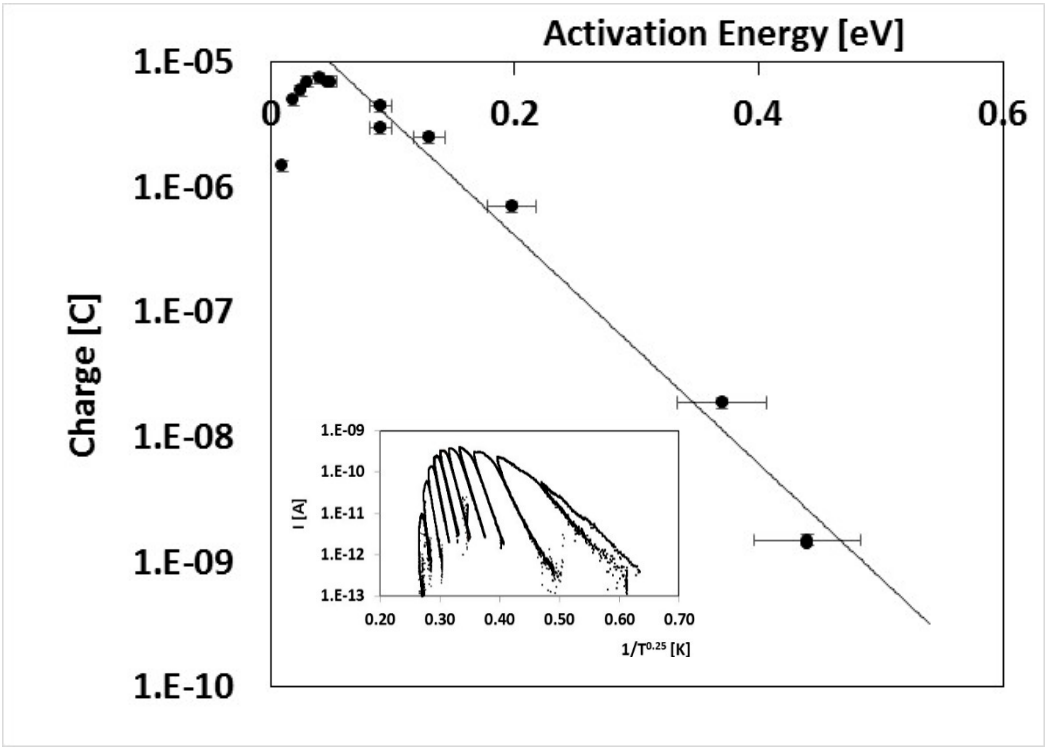

Figure 5. Emitted charge plotted as a function of the activation energy measured in the rising range of each peak of the fractionated TSC experiment shown in the inset. The exponential fit reflects the trend of the band tail in the deepest range within the forbidden gap. Inset: Delayed TSC in the range 5-150K plotted as a function of $1/T^{1/4}$ to evidence the contribution of hopping conduction in the electrical transport.

Preprints (www.preprints.org) | NOT PEER-REVIEWED | Posted: 1 November 2017 doi:10.20944/preprints201711.0002.v1

Peer-reviewed version available at Nanomaterials 2018, 8, 13; doi:10.3390/nano8010013

Best fit gives: E_L = 47.5meV, Q_L = 2.8 x 10^{-5} C, values fairly in agreement with literature [19]. We note that in the low energy range of the plot, the charge is lower than the expected value indicated by the exponential trend. This can be explained considering that priming could not fill all the states in the highest part of the band tail, close to the boundary point at ε = 0. As a strong evidence of this, using a deeper UV LED (355nm) the drop appears for shallower energies with respect to the shallower UV LED (400nm). Considering a 2mm diameter light spot and a sample thickness of about 1μm, the effective volume involved in this process is: $Vol \approx \pi \cdot 10^{-12}$ m^3 and a rough estimate of the density of states is: $N_L = \frac{Q_L}{qVol} \approx 5 \times 10^{19}$ cm^{-3}.

Best-fit of TSC experimental data shown in figure 4 in the low temperature range, obtained using our mixed conductivity model taking care of the band tail in the range down to 0.6eV plus a discrete level at 0.8eV, is shown in Fig. 6. Of note the agreement between numerical and experimental data in the overall range, up to almost 4 orders of magnitude of the current. A disagreement is observed at high temperature, where the experimental current stabilize itself on the pAs range, while in the numerical model it decreases to lower values, as a consequence of the decrease of the Fermi level towards midgap. The pAs contribution to the current could be due to the residual presence of water vapor physisorbed on the film surface, as discussed in the next section.

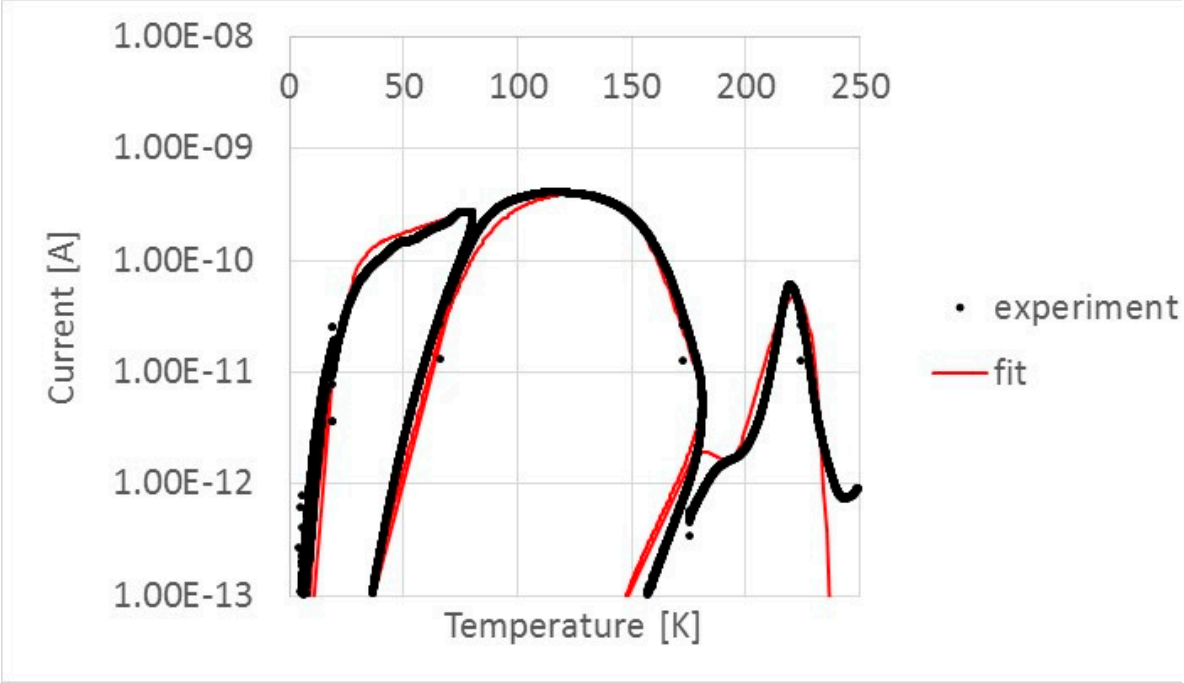

Figure 6. Experimental TSC measured in the 5-250K range and best fit obtained considering the mixed conductivity model taking care of both hopping and free carriers conduction plus emission from a discrete energy level at 0.8eV.

5.2. TSC analysis above room temperature

In this temperature range, the effect of hopping conduction should become more and more negligible against free carrier one. Moreover, physisorption and chemisorption mechanisms at surface should also participate to conduction. In particular, dangling bonds at the nc-TiO_2 surface are capturing and releasing oxygen depending on pressure and relative humidity, these effects should be possibly investigated separately. To this purpose, we performed different sets of measurements as follows.

5.2.1. Current vs Temperature with no priming

Measurements are performed without previous priming. Using a low heating/cooling rate (0.1K/s) as a first approximation we can assume a quasi-stationary equilibrium. The sample is kept in

dark with air at a pressure of 1100mb, slightly higher than ambient pressure. A typical measurement is presented in Fig. 7.

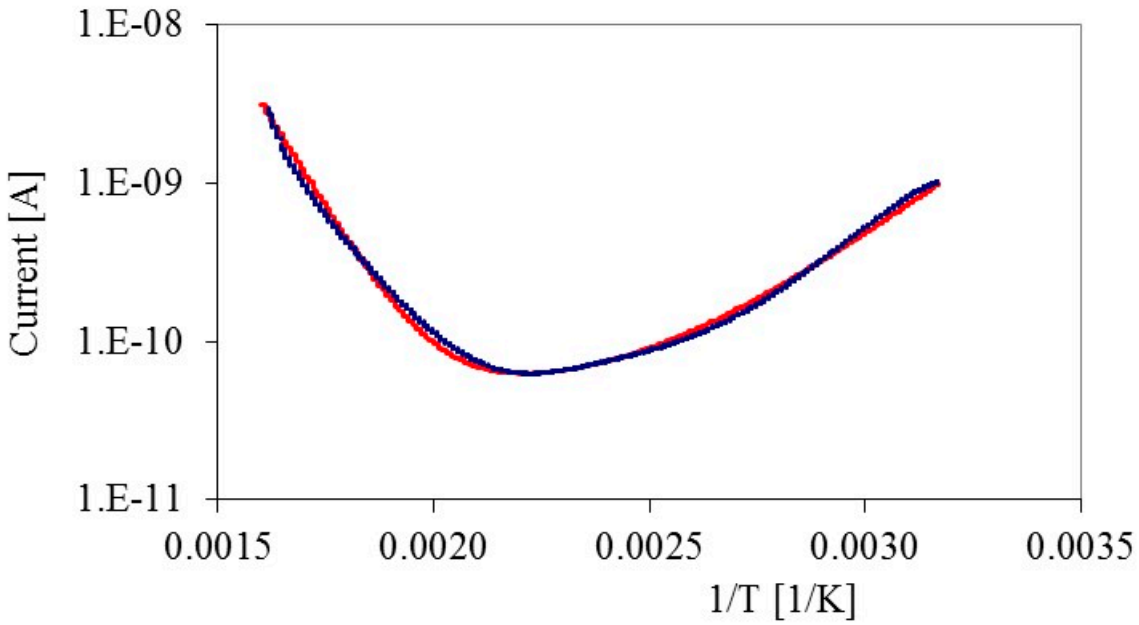

Figure 7. Current measured as a function of reciprocal temperature during a quasi-stationary heating process, in the range 300-600K with no priming. dark: data, red: best-fit.

The Arrhenius plot shows two distinct ranges: up to about 400K the current decreases increasing the temperature T, then it increases with T. To explain this behavior we can consider the model proposed by [22], taking account of two dominant defects, one acting as a trap, the other as a recombination center (probably associated to dangling bonds at surface, releasing holes via a thermally activating process). Neglecting the small contribution of the hopping, the rate equation for the charged carriers (free electrons and holes concentrations are denoted by n, p) is then given by:

$$\frac{dn}{dt} = N_{t1}c_1 e^{-E_{t1}/K_B T} - Bnp - (n - n_0)\gamma, \tag{17}$$

The first term of the right side is due to emission of electrons from the trap of energy E_{t1}, concentration N_{t1} and frequency factor c_1. The second term describes the recombination of electrons with holes at the recombination center. We here assume that also hole capture is a thermally activated process: $p = N_{t2}c_2 e^{-E_{t2}/K_B T}$, with N_{t2}, E_{t2}, c_2 respectively concentration, energy and frequency factor of the recombination center and B a probability coefficient. The third term in eq. (17) takes account of other possible free electron removal mechanisms, with a coefficient γ, as trapping from deeper levels.

During the current temperature measurements in dry fluxed air the system, is actually in a quasi-stationary regime, so we can reasonably consider $\frac{dn}{dt} = 0$, then:

$$n = \frac{n_0 + \frac{N_{t1}c_1}{\gamma} e^{-\frac{E_{t1}}{K_B T}}}{1 + \frac{BN_{t2}c_2}{\gamma} e^{-\frac{E_{t2}}{K_B T}}}, \tag{18}$$

which gives a current dependence with temperature as:

$$I_{fit} = \left(\frac{a + be^{-\frac{E_{t1}}{K_B T}}}{1 + de^{-\frac{E_{t2}}{K_B T}}} \right) \mathrm{F}, \tag{19}$$

Preprints (www.preprints.org) | NOT PEER-REVIEWED | Posted: 1 November 2017 doi:10.20944/preprints201711.0002.v1

Peer-reviewed version available at Nanomaterials 2018, 8, 13; doi:10.3390/nano8010013

with $a = q\Sigma\mu_c n_0; b = q\Sigma\mu_c \frac{N_{t1}c_1}{\gamma}; d = \frac{BN_{t2}c_2}{\gamma}$ and where again Σ is the surface normal to electric field F. Best-fit of our data with Eq. 19, shown in Figure 7, is obtained with energy values: E_{t1} = 1.30 ± 0.05eV and E_{t2} = 0.40 ± 0.05 eV.

5.2.2. TSC after storage in dark and humid environment

To analyze the effect of water vapor on TSC data, we first primed the sample by keeping it in a controlled humid environment (rh =20%) in dark at room temperature (T = 300K) for selected time intervals, up to 14 days. Then, a TSC heating/cooling cycle has been performed by fluxing dry air with a pressure slightly higher than atmosphere, in view to measure only emissions originated during charging in the storage period. As an example, Figures 8(a, b) show TSC experimental data obtained after 2 and 4 days storage respectively. TSC emissions are observed within two distinct ranges of temperatures: one from ambient temperature, up to 400K, the other one above 400K.

An evaluation of the main TSC components involved in these measurements has been carried out in order to identify the origin of the emissions. Measurements show statistically broadened emissions like the ones in Figures 8(a, b). They can be fitted using TSC peaks convoluted with a gaussian as given in Eq. 13. Best fits have been obtained by opportunely changing trap concentration N_t for a same set of $(E_t, \sigma_{E_t}, \sigma_n)$, within errors, best fitting the two measurements. Up to seven energy levels are required to fit our data. Parameters are shown in Table 1, energy levels are peaked at E_{to} = 0.7-1.14eV and are characterized by an energy spread σ_{E_t} up to 70meV. As a general trend, increasing the storage time, peaks at low temperatures decrease their concentration N_t, while those at high temperatures increase N_t. A source of uncertainty in the determination of concentration for the peak at ambient temperature is due to the increasing background current observed during the cooling stage, observed especially in Figure 8(a). This effect can indicate reversible charging/discharging of the involved energy states, maybe due to adsorbing/ desorbing from the porous alumina substrate.

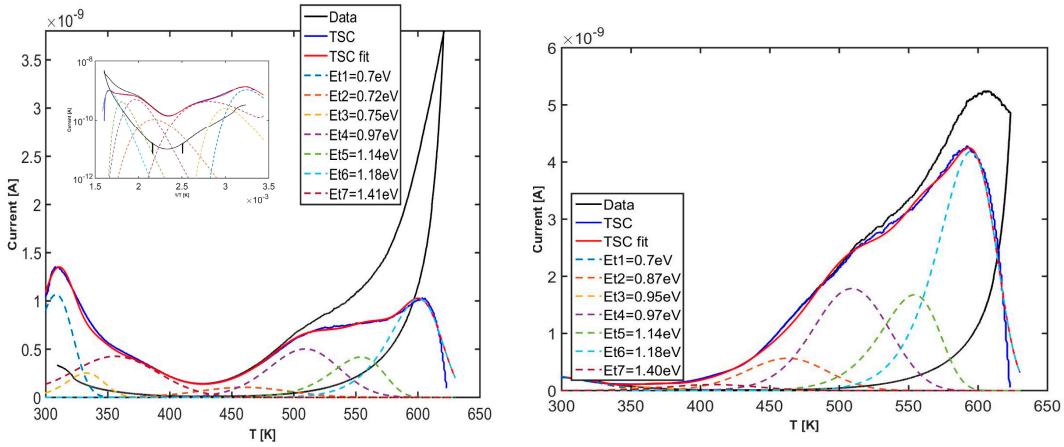

(**a**) (**b**)

Figure 8. TSC after storage in ambient air (T = 300K) in humid environment (rh = 20%) for (a) two days (inset: logarithmic plot) experimental data (black); TSC with background subtracted (blue); TSC best fit (red curve) obtained with a set of 7 peaks with energy E_{t0} given in the legend. (b) TSC measurements after four days storage and best fit with same E_{t0} parameters as in (a).

To comment on the origin of these peaks, we observe that our measurements are in agreement e.g. with temperature programmed desorption (TPD) analyses measured in past with TiO_2 after exposure to water. Four peaks at 155K, 190K, 295K, and 490–540 K were observed by [24,25], the first three assigned to molecular desorption from multilayer,

second layer, and first layer states, while the higher temperature feature was assigned to recombinative desorption. Effusion peaks from water were also observed in [26] by thermal desorption in the 150-350K range from porous nanostructured TiO_2 and attributed to physiosorbed H_2O, while in [27], two H_2O effusion peaks were detected around 440K and 650K. Moreover, physically adsorbed and dissociated H_2O molecules in nanostructured anatase TiO_2 have been studied by FTIR emission spectroscopy (IES) at different temperatures in the range 100-300 °C [28]. A 3665 cm^{-1} band assigned to OH hydrogen bonded (adjacent) OH groups was observed to considerably decrease when the sample was heated from 373K to 573K, while one at 3705 cm^{-1}, attributed to isolated OH groups, more difficult to remove from the surface than adjacent OH groups, only slightly changed. A 3250 cm^{-1} component attributed to the stretching vibration of water molecules that are hydrogen bonded was considerably weakened when heated up to 423K, while the one at 3400 cm^{-1}, related to hydrogen-bound surface OH groups (Ti OH), became visible at this temperature. This latter and the 1625 cm^{-1} band (identified as the water bond-bending vibration mode) finally disappeared at 573K. In our measurements, increasing the storage time, peaks at low temperature are decreasing, while those at high temperature are increasing, and eventually saturating. This can be explained considering that molecular adsorbed water, in time, is slowly evolving into recombinative species.

Table 1. Best fit trap parameters of the TSC measured after storage in humid air environment at room temperature

peak #	E_t [eV]	σ_{Et} [eV]	σ_n [cm^2]	N_t [$10^{16}cm^{-3}$] 2 days	N_t [$10^{16}cm^{-3}$] 4 days
1-3	0.70-75	0.070	10^{-20}-10^{-18}	0.34	0.06
4	0.97	0.070	$4x10^{-20}$	0.42	0.07
5	1.14	0.020	$2x10^{-19}$	0.3	1.43
6	1.18	0.007	$5x10^{-20}$	0.82	1.15
7	1.41	0.007	$7.x10^{-19}$	0.25	1.14

5.2.3. TSC after illumination in He atmosphere with different pressures

To evidence the effect on TSC of the oxygen-exchange at surface, we performed a set of measurements were the sample was primed in a dry He atmosphere at different pressure, from 10^{-6} bar to 1bar, at room temperature (T = 300K), during illumination with a Xe lamp for a selected time interval. Then, TSC heating/cooling cycles were carried out by fluxing dry air with a pressure slightly higher than atmosphere, to measure only emissions originated during charging in the storage period. In fact, it is known that oxygen vacancies can be created by annealing TiO_2 at elevated temperatures in an oxygen-poor environment, such as a pure He gas atmosphere or vacuum condition [29].

Results of photocurrent measurements during priming are shown in Fig. 9a. TSC curves after priming in these conditions are shown in Fig. 9b.

Preprints (www.preprints.org) | NOT PEER-REVIEWED | Posted: 1 November 2017 doi:10.20944/preprints201711.0002.v1

Peer-reviewed version available at Nanomaterials 2018, 8, 13; doi:10.3390/nano8010013

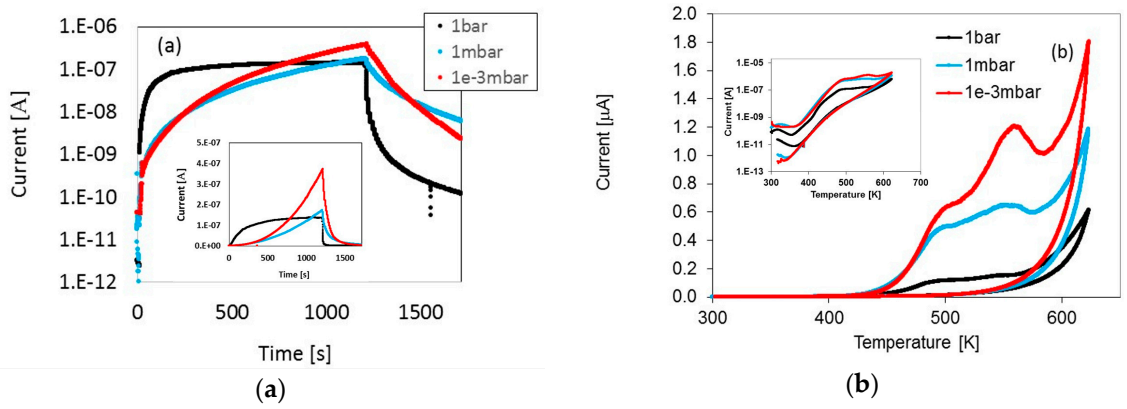

(a) (b)

Figure 9. (a) Photocurrent measured during priming by illuminating with a Xe lamp the nc-TiO_2 sample in an He atmosphere of different pressures at T = 300K. (b) TSC measured after priming with 1bar,1mbar, 10^{-3}mbar. Heating/cooling cycles are performed in He atmosphere with 1bar pressure.

While at 1bar the photocurrent is almost saturating during priming, at low pressure it increases superlinearly, a fact that can be explained considering the creation of extra oxygen-vacancies, which are releasing an ever increasing free carriers concentration, so favoring the passivation of deep traps during priming. To comment on TSC curves reported in Fig. 9b (inset: logarithmic plot) we observe that, in the case of vacuum priming, the tail in the cooling stage of increasing current below 400K observed in case of humid environment (Figures 7 and 8) is almost absent. Then, higher TSC emissions are observed in the high temperature range in vacuum, showing an increasing number of passivated deep traps in the priming stage. Best fits of the TSC measurements in He atmosphere have been performed starting with the same set of energy levels used in the previous section. They are shown in figures 10(a-c). Measured emissions have been calculated considering TSC peaks statistically broadened as given in Eq. 13. Results are shown in Figures 10(a,b,c) respectively for the cases of 1bar, 10^{-3}bar, 10^{-6}bar. Best-fit procedure turns out in a six-fold emission, with trap parameters listed in Table 2. The fit has been performed considering the same set of values (E_t, σ_{E_t}, σ_n), within errors, for the three measurements, and best-fitting the TSC scans obtained by subtracting the response during cooling to the one measured during heating and by opportunely changing the trap concentration values N_t. Trap parameters given in table 2 are in agreement with the model [30] indicating that localized donor states originating from oxygen vacancies are located at 0.75–1.18 eV below the conduction band of Titania.

Table 2. Best fit trap parameters of the TSC measured after storage in different pressures of He atmosphere at room temperature during illumination with a Xe lamp.

peak #	E_t [eV]	σ_{Et} [eV]	σ_n [cm^2]	N_t [$10^{18}cm^{-3}$] 1bar	N_t [$10^{18}cm^{-3}$] 10^{-3} bar	N_t [$10^{18}cm^{-3}$] 10^{-6} bar
1	0.750	0.040	$1x10^{-18}$	$1.8x10^{-4}$	$0.7x10^{-3}$	$0.5x10^{-3}$
2	0.870	0.001	$3x10^{-18}$	$0.4x10^{-4}$	$0.2x10^{-3}$	$0.3x10^{-3}$
3	1.031	0.015	$3x10^{-20}$	0.31	1.35	1.35
4	1.166	0.030	$1x10^{-18}$	0.37	1.53	1.08
5	1.177	0.007	$5x10^{-20}$	0.38	2.87	6.21
6	1.411	0.009	$7x10^{-19}$	0.94	2.88	4.77

The six peaks used to best-fit our TSC curves are characterized by the same (E_t, σ_{Et}, σ_n), within errors, used to fit TSC measurements in the humid environment (apart of the shallowest two levels that here are present in only one component). Here, at every pressure analyzed, shallowest levels have negligible concentrations with respect to deepest levels. Looking to plots in Figures 10, we observe a good agreement between fit and data on a four-orders of magnitude scale. Logarithmic

Preprints (www.preprints.org) | NOT PEER-REVIEWED | Posted: 1 November 2017 doi:10.20944/preprints201711.0002.v1

Peer-reviewed version available at Nanomaterials 2018, 8, 13; doi:10.3390/nano8010013

plots are shown as a function of 1/T: the observed linear trend is in favour with our previous observation, that hopping conduction in this high-temperature range is negligible.

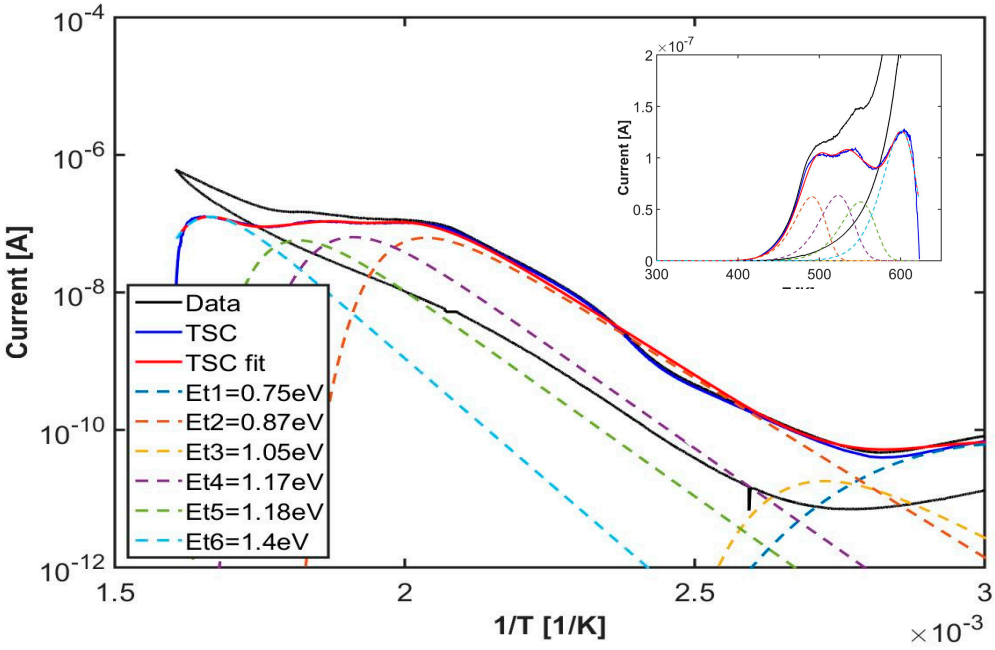

(**a**)

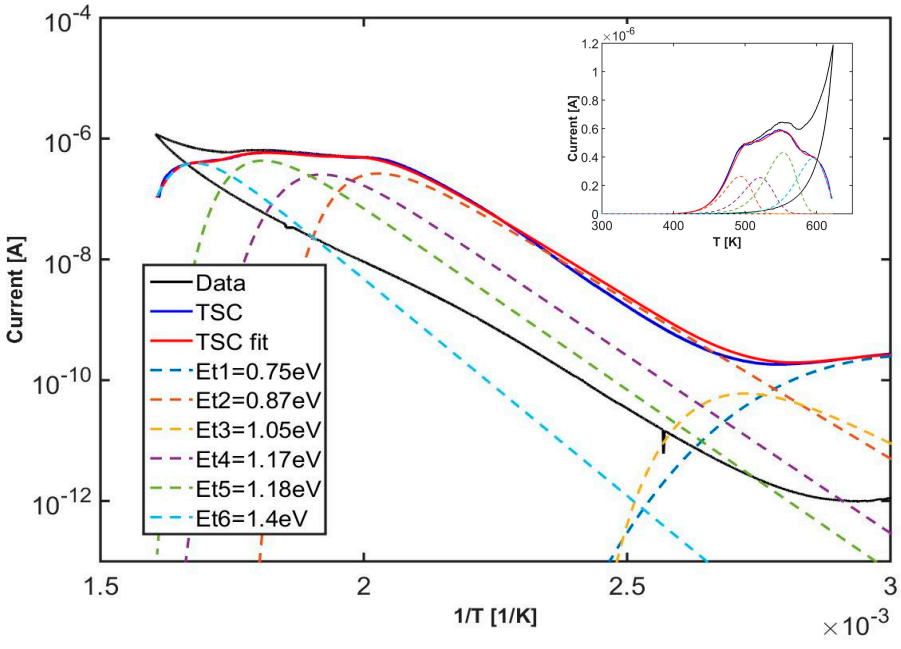

(**b**)

Peer-reviewed version available at Nanomaterials 2018, 8, 13; doi:10.3390/nano8010013

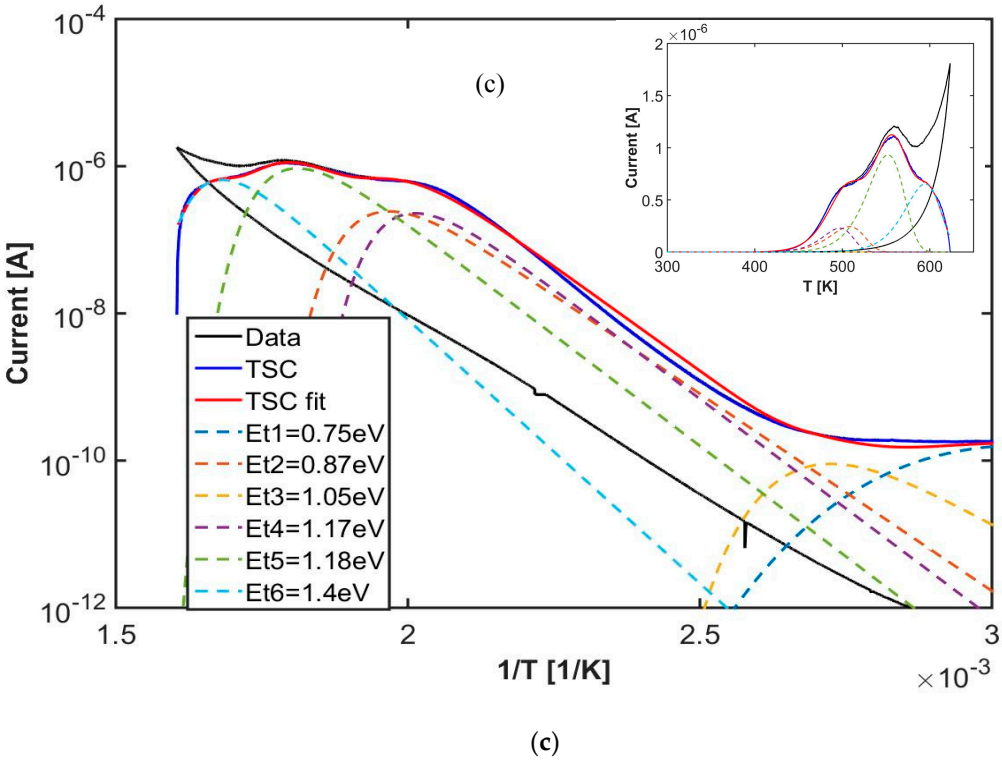

(c)

Figure 10. TSC response after priming in He atmosphere with a pressure in chamber (a) 1bar; (b) 10^{-3} bar (c) 10^{-6} bar. TSC experimental data (black); Blue: TSC heating scan subtracted from background (cooling stage); dotted curves: TSC peaks convoluted with a gaussian, parameters are given in table 2.

6. Conclusions

Nanocrystalline Titanium dioxide is widely applied as a high gap semiconducting material in many optoelectronic devices, from solar cells to gas sensors, where its peculiar electronic properties and high chemical reactivity play a crucial role. To attain good performances in terms of efficiency and photoactivity, Titania is mostly used in form of porous nanocrystalline thin films, a material characterized by a high degree of microstructural disorder, which detrimental effect in transport properties should be taken in great care and possibly minimized.

The thermally stimulated current technique is one of the most effective tool for characterizing electrical defects in semiconductors. In this paper, we have used this method to get an overall picture of the defect distribution in nanocrystalline Titania used in state-of-art DSSC devices. The model of TSC used to interpret our experimental results, briefly described in this work, takes account of the heavily disordered microscopic nature of nc-TiO_2. Mixed conductivity with non-negligible contributions from hopping between localized defects grouped in a band-tail below the conduction band is considered. Moreover, a broadening of the energy levels associated to discrete defects in the forbidden gap, has been accounted for, by convoluting the TSC standard emission with a gaussian distribution. Shallow-to deep energy level ranging from 0.1eV to 1.4eV have been studied via a thermal spectroscopy spanning from 5K to 630K and interpreted with this model: main results of our analysis can be summarized as follows.

An exponential DoS tail within the forbidden gap has been observed in the range 0.1-0.6eV from the bottom of the conduction band, with energy tailing factor of about 47.5meV, characterized by density of states of the order of $10^{20}cm^{-3}$. This tail is responsible for a large TSC emission visible after priming with a UV source at 5K for temperatures up to approximately 150K. At higher temperatures, up to room temperature and above, the hopping contribution to conduction becomes less and less negligible against free carrier one and contributions from discrete energy levels emitting in the conduction band become visible. Similar to single crystal TiO_2, a sharp TSC peak at 220K is observed,

with energy 0.8eV, probably related to water adsorption. Above room temperature, dark current measured as a function of the temperature without any priming reveals to be non-negligible, as it should be due in pure intrinsic TiO_2 material. So, we studied it separately before any TSC analysis. Measurements as a function of temperature shows a double exponential trend, with a minimum at about 400K. To explain this behavior a model taking account of two dominant defects, one acting as a recombination center, the other as a trap has been considered. The activation energy measured in this experiment in dark, for the recombination center, is about 0.4eV a value compatible with dangling bonds at surface [23]. The trap energy, evaluated as about 1.3eV, is in the highest energy range found for trap states observed in our further analyses.

Then, TSC response above background current has been studied as a function of the temperature, as a spontaneous emission observed after a prolonged storage of the sample in moderately (rh=20%) humid ambient air. They are best-fitted using gaussian-broadened TSC emissions, with average energy 0.7-1.4eV, characterised by uncertainties up to 70meV. Two groups of peaks are measured, respectively below and above temperature. Peaks up to 350K are probably related to molecular desorption from multilayer, second layer, and first layer states, while the higher temperature features should be assigned to recombinative desorption [31]. Our measurements show that increasing the storage time molecolar adsorbed water slowly evolves into recombinative species. Finally, to evidence the relationship between TSC emissions and vacancy-oxygen defects, measurements have been carried out after priming in inert atmosphere (He) at different pressures. Main TSC emissions, observed in the high temperature range, 400-630K, are best-fitted considering energy levels for localized energy states in the range 0.75–1.18 eV, in agreement with a model from [28] for donor states related to oxygen-vacancies below the conduction band.

Acknowledgments: Authors wish to heartily acknowledge Prof. Franco Bogani, from University of Florence (now retired) for helpful discussions and precious guidance . This study has been performed within the SEAR laboratory of CERTUS, University of Florence.

References

1. Gratzel, M. Dye-sensitized solar cells. *J. Photochem. Photobiol.C* **2003**, 4, 145-153, https://doi.org/10.1016/S1389-5567(03)00026-1.
2. Lin, H.-M.; Keng, C.-H.; Tung, C.-Y. Gas-sensing properties of nanocrystalline TiO2. *Nanostructured materials* **1997**, 9, 747-750, https://doi.org/10.1016/S0965-9773(97)00161-X.
3. Gu, B.; Xu, Z.; Dong, B. A theoretical interpretation of thermostimulated conductivity in amorphous semiconductors. *J. Non-Cryst. Solids* **1987**, 97-98, 479-482, https://doi.org/10.1016/0022-3093(87)90112-8.
4. Bruzzi, M.; Mori, R.; Carnevale, E.; Scaringella, M.; Bogani, F. Low temperature Thermally Stimulated Currents (TSC) characterization of nanoporous TiO2 films. *Phys. Status Solidi A, 2014*, 211, 1691-1697, http://dx.doi.org/ 10.1002/pssa.201330608.
5. Baranovski, S. D.; Zhu, M.; Faber, T.; Hensel, F.; Thomas, P.; von der Linden, M. B. and van der Weg, W. F. Thermally stimulated conductivity in disordered semiconductors at low temperatures. *Phys. Rev. B* **1997**, 55, 16227-16232, https://doi.org/10.1103/PhysRevB.55.16226.
6. Nagy, A.; Hundhausen, M.; Ley, L.; Brunst, G.; Holzenkämpfer, E. Steady-state hopping conduction in the conduction-band tail of a-Si:H studied in thin-film transistors, *Phys. Rev. B* **1995**, 52, 11289-11295, https://doi.org/10.1103/PhysRevB.52.11289.
7. Bube, R. H. *Photoelectronic properties of semiconductors*, 1st ed.; Cambridge University Press: Cambridge., Great Britain, 1992; pp. 171, ISBN 0-521-40491-6.
8. U.Diebold, Perspective: A controversial benchmark system for water-oxide interfaces: H2O/TiO2(110), The Journal of Chemical Physics, 2017, 147, 040901.
9. M. Setvin, J. Hulva, G. S. Parkinson, M. Schmid, U. Diebold,Electron transfer between anatase TiO2 and an O2 molecule directly observed by atomic force microscopy, Proceedings of the National Academy of Science of the United States of America, 2017, 114, 13, E2556–E2562.
10. Tiedje, T.; Cebulka, J. M.; Morel, D. L.; Abeles, B.. Evidence for exponential band tails in amorphous silicon hybride. *Phys. Rev. Lettters*, **1981**, 46, 21-25, https://doi.org/10.1103/PhysRevLett.46.1425.

11. Miller, A.; Abrahams, E. Impurity Conduction at Low Concentrations. *Phys. Rev.*, **1960**, 120, 745-755, https://doi.org/10.1103/PhysRev.120.745.
12. Shklovskii, B.I.; Efros, A.L. *Electronic Properties of doped Semiconductors*, 1st ed.; Springer-Verlag: Heidelberg, Germany, 1984; ISBN 978-3-662-02403-4.
13. Bak, T.; Nowotny, J.; Rekas, M.; Sorrell, C. C. Defect chemistry and semiconducting properties of titanium dioxide: III. Mobility of electronic charge carriers. *Journal of Physics and Chemistry of Solids* **2003,** 64, 1069–1087, https://doi.org/10.1016/S0022-3697(02)00481-X.
14. Yagi, E.; Hasiguti, R. R.; Aono, M. Electronic conduction above 4 K of slightly reduced oxygen-deficient rutile TiO2-x. *Phys. Rev. B*, **1996**, 54, 7945-7956, https://doi.org/10.1103/PhysRevB.54.7945.
15. Steiger, J.; Schmechel, R.; von Seggern, H. Energetic trap distributions in organic semiconductors. *Synthetic materials*, **2002**, 129, 1-7, https://doi.org/10.1016/S0379-6779(02)00012-7.
16. Blood, P.; Orton, J. W. *The Electrical Characterization of Semiconductors: Majority Carriers and Electron States*, 2st ed.; Academic Press: London, Great Britain, 1992; pp. 393-397 and pp. 469–473, ISBN 9780125286275.
17. Mori, R.; Scaringella, M.; Cavallaro, A.; Bogani, F.; Bruzzi, M. Low temperature thermally stimulated current analysis of nanocrystalline Titanium dioxide. In PoS, Proceedings of the Conference 10th International Conference on Large Scale Applications and Radiation Hardness of Semiconductor Detectors-Rd11, PoS: Florence, Italy, 2011.
18. Baldini, A.; Bruzzi, M. Thermally stimulated current spectroscopy: Experimental techniques for the investigation of silicon detectors. *Rev. Scient. Instr.*, **1993**, 64, 932-936, http://dx.doi.org/10.1063/1.1144145.
19. Wakim, F. G. Some effects of trapping on the Photoelectronic properties of TiO2 single crystals. *Phys. Stat. Sol. A*, **1970**, 1, 479-485, http://dx.doi.org/10.1002/pssa.19700010313.
20. Baranovski, S.; Rubel, O. Description of Charge transport in amorphous semiconductors. In *Charge transport in Disordered Solids with applications in Electronics*, 1st ed.; Baranovski, S.; John Wiley & Sons: Chichester, UK, 2006; pp. 61, http://dx.doi.org/10.1002/0470095067.ch2.
21. Van de Lagemaat, J.; Frank, A.J. Nonthermalized Electron Transport in Dye-Sensitized Nanocrystalline TiO2 Films: Transient Photocurrent and Random-Walk Modeling Studies. *J. Phys. Chem. B*, **2001**, 105, 11194-11205, http://dx.doi.org/ 10.1021/jp0118468.
22. Nelson, J.;Eppler, A. M.; Ballard, I. M. Photoconductivity and charge trapping in porous nanocrystalline titanium dioxide. *J. Photochemistry and Photobiology A*, **2002**, 148, 25-31, https://doi.org/10.1016/S1010-6030(02)00035-7.
23. Weiler, B.; Gagliardi, A.; Lugli, P. Kinetic Monte Carlo Simulations of Defects in Anatase Titanium Dioxide. *J. Phys. Chem. C* **2016**, 120, 10062−10077, https://doi.org/10.1021/acs.jpcc.6b01687.
24. M. A. Henderson, Langmuir 12, 5093 (1996).
25. M. A. Henderson, S. Otero-Tapia, and M. E. Castro, Faraday Discuss. 114, 313 (1999).
26. Diebold, U. The surface science of titanium dioxide. *Surface science reports*, **2003**, 48, 59-229, https://doi.org/10.1016/S0167-5729(02)00100-0.
27. Weidmann, J.; Dittrich, Th.; Kostantinovac, E.; Lauermann, I.; Uhlendorfa, I; Koch, F. Influence of oxygen and water related surface defects on the dye sensitized TiO2 solar cell. *Solar Energy Materials and Solar Cells*, **1999**, 56, 153 -165, https://doi.org/10.1016/S0927-0248(98)00153-6.
28. Zhanfeng Zheng et al. Correlation of the Catalytic Activity for Oxidation Taking Place on Various TiO_2 Surfaces with Surface OH Groups and Surface Oxygen Vacancies, Chem. Eur. J. 2010, 16, 1202 – 1211
29. Xiaoyang Pan,et al. Defective TiO2 with oxygen vacancies: synthesis, properties and photocatalytic applications, Nanoscale, 2013, 5, 3601.
30. I. Nakamura, N. Negishi, S. Kutsuna, T. Ihara, S. Sugihara and K. Takeuchi, J. Mol. Catal. A: Chem., 2000, 161, 205
31. I. M. Brookes, C. A. Muryn, and G. Thornton, Imaging Water Dissociation on TiO_2 (110), Phys. Rev. Lett., 2001, 86, 26, 266103-1,.